Reports

Heavy-Particle Radiography

Abstract. *Energetic heavy particles from an accelerator may be used to produce radiographs with high contrast and high depth resolution. Small differences in the stopping power of objects can be detected and permanently recorded by using stacks of plastic track detectors. This method should aid in the diagnosis of soft-tissue abnormalities, including some tumors, and make possible quantitative reconstruction of the internal density structure of objects.*

The failure of x-ray diagnostic techniques to accurately detect tumors and other regions of abnormal density in soft tissue has been, for many years, a significant shortcoming of this important technique in medicine. In this report we show that the use of monoenergetic heavy particles produced in an accelerator, in combination with thin-sheet plastic track detectors, will considerably extend the possibility of detecting soft-tissue abnormalities and localizing air pockets, and may make possible the detection of small metastatic lesions invading bone. In addition, we show that these are also improvements over the diagnostic potential of protons.

For radiography, the advantage of heavy ions over x-rays, neutrons, or electrons is that there are precise range-energy relations for heavy ions, which makes them a more sensitive "thickness gauge" (*1*). Also, the range of heavy ions is primarily sensitive to the density of the specimen, whereas in the attenuation of x-rays the chemical composition is more significant. Accelerated protons have already been used in radiography (*2*). The advantage of heavier ions over protons lies in the lower dose required to produce radiographs, and in that heavy particles undergo less scattering and range straggling and therefore make possible greater spatial resolution. For example, a soft-tissue tumor 1 cm in diameter, with a 5 percent density difference, provides a relative displacement of the beam stopping point of only 0.5 mm of water. If it occurs somewhere within a body, the particle range may be between 20 and 30 cm. For ranges this large, particles at least as heavy as ^{16}O must be used if the range straggling is to be sufficiently small (about 0.5 mm or less) that the beam displacement can be resolved.

Initial studies were carried out by using the ^{16}O ion beam (approximately 250 Mev/nucleon) of the bevatron at Lawrence Berkeley Laboratory (*3*). The particles have a range of nearly 10 cm in tissue, and their energy is degraded by allowing them to pass through several centimeters of water. They then penetrate the target specimen, and finally are recorded on either photographic film or plastics placed downstream and adjacent to the specimen. In the most common case, where the main interest is in obtaining the internal density distribution of a specimen, the effect of the external geometry (shape) of the specimen is minimized by immersing it in water.

Emphasis has been on using plastic track detectors since they offer some unique advantages over photographic film. The main limitations of photographic film are that it has a logarithmic response; records electrons, producing an unwanted halo effect; and records all the charged secondaries. Plastics are inexpensive detectors which are sensitive to position and energy (*4*). Since they are essentially threshold type detectors, they are unaffected by electrons and light secondaries, and record tracks only near the point where a particle comes to rest.

Each layer of an exposed stack of plastic detectors may have unique information permanently recorded on it. The information is in the form of a two-dimensional segment (picture) of the overall three-dimensional density distribution. Thus, it is possible to detect very small variations in the stopping power and to reconstruct the three-dimensional structure of the target object by using a suitable technique, such as particle laminography (*3, 5*).

Depending on the exact end point desired, a variety of techniques can be used to process and analyze the data. For example, the detector processing method can be selected to achieve the desired detector sensitivity. The processed detectors can be analyzed either by computer or by photographing the individual layers. With the computer techniques the feature contrast can be enhanced essentially by subtracting in-

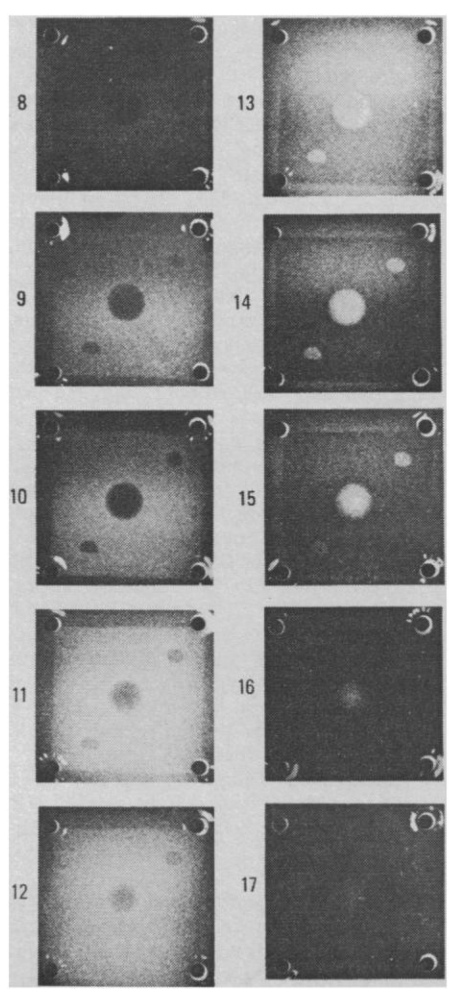

Fig. 1. Ten-layer Lexan radiographic sequence, produced by ^{16}O particles, of a spherical cavity, 1 cm in diameter, in Lucite. The cavity is filled with a sucrose solution 5 percent lower in density than the Lucite.

Scoreboard for Reports: In the past few weeks the editors have received an average of 68 Reports per week and have accepted 12 (17 percent). We plan to accept about 12 reports per week for the next several weeks. In the selection of papers to be published we must deal with several factors: the number of good papers submitted, the number of accepted papers that have not yet been published, the balance of subjects, and length of individual papers.

Authors of Reports published in *Science* find that their results receive good attention from an interdisciplinary audience. Most contributors send us excellent papers that meet high scientific standards. We seek to publish papers on a wide range of subjects, but financial limitations restrict the number of Reports published to about 15 per week. Certain fields are overrepresented. In order to achieve better balance of content, the acceptance rate of items dealing with physical science will be greater than average.

formation recorded on the adjacent detector layers. The photography of individual layers can also be varied to adjust the "latitude" of the detector, for example by using either incident light scattered by all the recorded tracks or light that is exclusively transmitted by the track-produced holes.

Although the heavy-ion bevatron beam is only in its initial stages of development, radiographic studies have shown that density changes as small as 0.03 g/cm^2, or about 0.3 percent of the total thickness, in regions of relatively small size (less than 1 cm in diameter) can be detected with ease. Two of the available plastic track detectors have been used: cellulose nitrate (CN) and Lexan. Of the two, the CN detector is more sensitive and therefore offers a greater latitude. The radiographs produced with this detector have the more standard appearance of conventional x-ray pictures. Lexan, having a higher threshold, offers a much narrower latitude. Its response closely approximates the actual distribution of particle stopping-points. This detector is most useful in situations involving detailed reconstructions of density distributions.

Figures 1 to 3 illustrate the results obtained with the ^{16}O particle beam with Lexan and CN detector sheets 0.25 mm thick assembled into stacks. All the detectors were processed in a 6.25*N* NaOH solution with etch times and temperatures of 8.0 hours at 70°C for Lexan, and 4.0 hours at 40°C for CN. In all of the figures the numbers on the left correspond to the detector layer number, with layer 1 being upstream of the others.

Figure 1 shows a ten-layer Lexan radiographic sequence of a model tumor which consists of a Lucite block containing a spherical cavity, 1 cm in diameter, filled with a sucrose solution 5 percent lower in density than the block. Two small air bubbles are situated almost diagonally with respect to the square plastic. The bubbles are about 5 mm in diameter and represent a thickness change of about 0.03 g/cm^2. The outline of the paper gasket used to seal the two halves of the Lucite block is also visible in Fig. 1. This represents an even smaller thickness change than that for the air bubbles.

Figure 2 shows a four-layer CN radiographic sequence of a 14-day-old chicken egg containing an embryo. The picture on the right is a 35-kv x-ray of the same egg. Whereas in the x-ray some bone structure is just distinguishable (even less is visible at the standard higher voltages), the plastic radiographs show considerable detail in the distribution of the soft tissue; the head of the embryo is located on the left. The white appearance (tracks) of the embryo in layer 1 also shows that it has a slightly higher density than the surrounding material. The spots appearing on the periphery of the egg are due to air bubbles trapped in a piece of foam rubber used to hold the egg under water. The "negative" character of the image produced in layers 6 and 7 compared with that in layers 1 and 2 results from their situation on opposite sides of the peak of the particle stopping-point distribution.

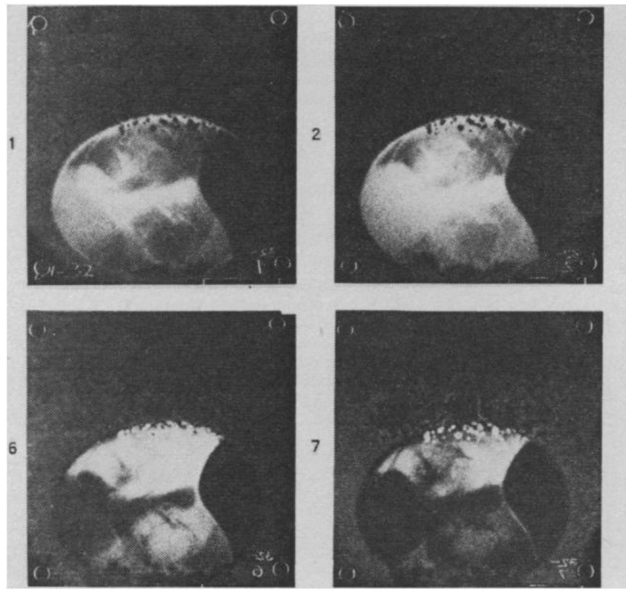

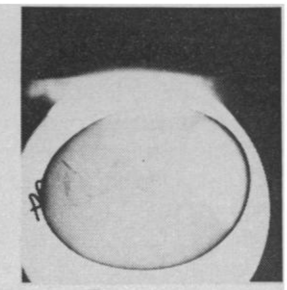

Fig. 2. Four-layer CN radiographic sequence, produced by ^{16}O particles, of a 14-day-old fertilized chicken egg. The x-ray on the right (optimum conditions) was taken with: focus, 21 cm to Cronex film; potential, 35 kv; current, 50 ma; exposure time, 24 seconds; and inherent filtration, 0.8.

Figure 3 shows a seven-layer Lexan radiographic sequence of a tropical fish 4 cm long; an x-ray appears on the bottom right. A sharp, high-contrast image of the air bladder is observed, however the skeletal bone structure is not recorded. This illustrates how the technique complements x-ray radiography, and shows that this system of imaging depends on the total mass in the path of each particle rather than just on local density variations.

In all cases, the radiographs were obtained by using a single beam pulse of about 10^6 particles, corresponding to an absorbed dose of about 1 rad. Lower exposure levels (about 0.1 rad) still yielding high-quality radiographs can be obtained by enlarging the recorded tracks through a longer etch time. Since exposure times are very short, the technique can also be applied to obtain blur-free radiographs of biological specimens in motion.

Before this technique can become a practical tool in diagnostic radiography, a number of areas need clarification. We do know that density differences exist between various types of normal and tumor tissues, but practical applications to tumor diagnosis must be based on experience in each case, as is being done in experimental approaches to soft x-ray mammography (*6*). The restrictions imposed on sensitivity by (as yet

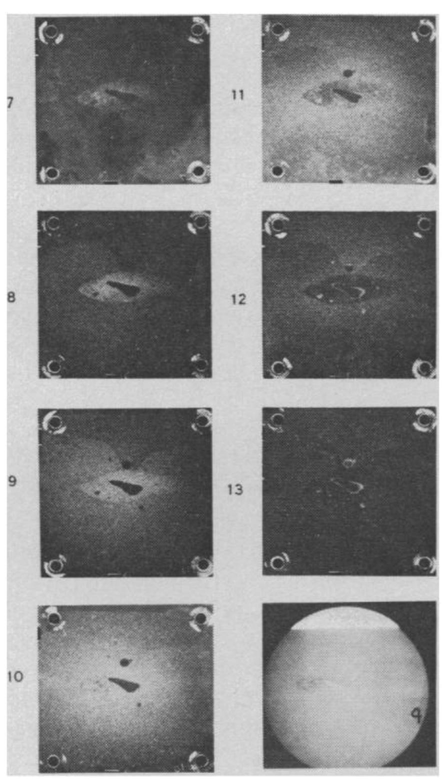

Fig. 3. Seven-layer Lexan radiographic sequence, produced by ^{16}O particles, of a tropical fish 4 cm long. The x-ray, shown on the right, was taken with the fish inside the water box under the same conditions as in Fig. 2, except that the exposure time was 1.5 seconds.

unknown) normal variations in tissue density need to be determined. Although the pictures already taken show that useful data can be obtained with water immersion, more work needs to be done on the effectiveness of water or other suitable liquids used to compensate for variations in body thickness. Nevertheless, it is clear that heavy particle beams probably represent the most sensitive tool presently available for the measurement of internal density distributions of objects. Indeed, the technique is general and is applicable in areas other than medicine.

E. V. BENTON
R. P. HENKE

Physics Department, University of San Francisco, San Francisco, California 94117

C. A. TOBIAS

Donner Laboratory, University of California, Berkeley 94720

References and Notes

1. C. A. Tobias, T. L. Hayes, H. D. Maccabee, R. M. Glaeser, *Report UCRL-17357* (University of California Radiation Laboratory, Berkeley, 1967), p. 108; C. A. Tobias and H. D. Maccabee, in *Elementary Particles: Science, Technology, and Society*, L. C. Yuan and C. S. Wu, Eds. (Academic Press, New York, 1971), chap. 5.
2. H. L. Anderson, U.S. Patent No. 2,953,510 (1960); A. M. Koehler, *Science* **160**, 303 (1968); D. West and A. C. Sherwood, *Nature* **239**, 157 (1972); V. W. Steward and A. M. Koehler, *Science* **179**, 913 (1973).
3. C. A. Tobias *et al., Science* **174**, 1131 (1971); E. V. Benton, R. P. Henke, C. A. Tobias, *Report LBL-2016* (Lawrence Berkeley Laboratory, Berkeley, Calif., 1973), p. 1.
4. R. L. Fleischer, H. W. Alter, S. C. Furman, P. B. Price, R. M. Walker, *Science* **178**, 255 (1972).
5. M. Goitein, *Nucl. Instrum. Methods* **101**, 509 (1972).
6. J. W. Boag, A. J. Stacey, R. Davis, *Brit. J. Radiol.* **45**, 633 (1972); A. H. Dowdy, W. F. Barker, L. D. Lagasse, L. Sperling, L. J. Zeldis, W. P. Longmire, *Cancer* **28**, 1558 (1971); R. L. Egan, *ibid.*, p. 1555.
7. We thank J. Lyman, J. Howard, G. Welch, D. Palmer, W. Shimmerling, R. Walton, J. McGinnis, and the bevatron crew at Lawrence Berkeley Laboratory for their generous help. This work is supported in part by the Atomic Energy Commission.

9 July 1973

State of Equilibrium of the West Antarctic Inland Ice Sheet

Abstract. *Data from a traverse connecting Byrd Station, Antarctica, with the local ice divide allow calculation of the mean volume flux at points along the traverse. This is compared with current rates of surface accretion upstream from each point. Near the ice divide the ice sheet seems to be in equilibrium, but near Byrd Station the volume flux is in excess of that needed for ice sheet equilibrium by at least 15 percent. The discrepancy may exist because the traverse does not follow the ice flow exactly or because ice flow at depth is very complex. Although neither of the foregoing possibilities can be disproved, it seems most likely that the discrepancy is due to ice sheet thinning, as has previously been suggested by work on oxygen isotope ratios and temperature in the boreholes at Byrd Station. This thinning probably started at the end of the Wisconsin/Würm glaciation. Causes for the thinning are discussed.*

The large Antarctic inland ice sheets have very low rates of movement and surface accretion which makes them very sluggish in response to climatic change. Measurements in central West Antarctica (Fig. 1) suggest that the ice sheet regime is not in equilibrium with the present climate, and that the ice sheet is thinning and that it is, at least in part, a relic of a former climate, probably that of the Wisconsin/Würm glaciation.

Surface mass balance, strain rates, and ice thicknesses have been obtained along a traverse upstream from Byrd Station, Antarctica (*1*). The traverse crosses the ice divide, and, by a process of successively adding balances and correcting for strains, it has been possible to calculate the equilibrium condition of this portion of the ice sheet.

Consider a small prism of ice (Fig. 2) bounded on two faces by flow lines and on two other faces by the top and bottom surfaces of the ice sheet. If the strain rate (measured only at the surface) does not vary with depth, equilibrium requires that, at a distance x from the ice divide

$$Q_{x+\Delta x}\,\bar{h}_{x+\Delta x}\,w_{x+\Delta x} = Q_x\bar{h}_x w_x + \tfrac{1}{2}(b_t + b_b)(w_x + w_{x+\Delta x})\Delta x \quad (1)$$

where Q_x is the equilibrium velocity at x or the mean velocity with depth needed for ice sheet equilibrium; Δx is the length of the prism; h_x is the mean ice thickness at x, taken to be constant in time; w_x is the spacing between flow lines at x; and b_t and b_b are the top surface and bottom balances, respectively.

For an ice sheet in perfect equilibrium, the amount of ice moving through a section is equal to the amount of snow accumulation upstream from the section plus or minus the amount of basal freezing or melting. All these quantities are expressed in equivalent volumes of ice. The volume flux density then has the units of a velocity (cubic meters per square meter per year or meters per year). This velocity has been called the "balance velocity" (*2*) but, as a reviewer (Dr. C. R. Bentley) has pointed out, this term is confusing and so I will use the term "equilibrium velocity." The nonequilibrium of the ice sheet is expressed by any difference in value between this theoretical equilibrium velocity, Q, and the actual velocity, $\bar{V}$, with the mean taken through the thickness of the ice sheet. In principle, the equilibrium velocity can be calculated by means of Eq. 1 and other simple relationships at any distance from the ice divide, where $Q_{x=0} = 0$.

The surface velocity, V, is found from the relative movements of poles along the traverse and the assumption that the crest of the ice sheet is also the ice flow divide. At the crest the surface slope is zero and there can be no horizontal gravity force gradients, and, hence, in the absence of significant longitudinal stresses or structural asymmetry, there can be no horizontal motion. Owing to internal shear, the measured V is greater than $\bar{V}$, and a correction must be applied.

The traverse, however, does not follow the flow line exactly, and it is necessary to work with components resolved onto the traverse axis. Let θ be the angle between the flow lines and the traverse axis. Then, with primed quantities being measured with respect to the traverse axis, the following equalities hold:

$$Q'_{x'} = Q_x \cos\theta$$
$$x' = x\cos\theta$$
$$\Delta x' = \Delta x\cos\theta$$
$$w' = w/\cos\theta$$

and let

$$\Delta w' = w'_{x'+\Delta x'} - w'_{x'}$$

From Eq. 1

$$Q'_{x'+\Delta x'} = \frac{Q'_{x'}\bar{h}_{x'} + (b_t + b_b)\left(1 + \tfrac{1}{2}\dfrac{\Delta w'}{w'_{x'}}\right)\Delta x'}{\bar{h}_{x'+\Delta x'}\left(1 + \dfrac{\Delta w'}{w'_{x'}}\right)}$$

where $\Delta w'/w'_{x'}$, the transverse strain, is equal to the transverse strain rate, $\dot{e}_{y'y'}$, times the time, t, taken to travel the distance $\Delta x'$,

$$\frac{\Delta w'}{w'_{x'}} = \dot{e}_{y'y'}\,t$$
$$t = \frac{\Delta x'}{\bar{V}'}$$